Ballistic impact on an industrial tank: Study and modeling of consequences

Nicolas Lecysyn, Aurélia Dandrieux, Frederic Heymes, Laurent Aprin, Pierre Slangen, Laurent Munier, Christian Le Gallic, Gilles Dusserre

Ballistic impact on an industrial tank: Study and modeling of consequences

Nicolas Lecysyn [a,*], Aurélia Dandrieux [a], Frédéric Heymes [a], Laurent Aprin [a], Pierre Slangen [a], Laurent Munier [b], Christian Le Gallic [b], Gilles Dusserre [a]

[a] *Ecole des Mines d'Alès 6, avenue de Clavières, 30319 Alès Cedex, France*
[b] *Centre d'études de Gramat, Délégation Générale pour l'Armement 46500 Gramat, France*

A B S T R A C T

We have studied the sequence of events that occurs when a high-speed projectile (from 960 m s^{-1} to 1480 m s^{-1}) penetrates a vessel filled with toxic liquid. We find that prior to liquid ejection several well-defined phases occur, including the phenomenon known as the "hydraulic ram." Then a catastrophic tank failure leads to liquid ejection and fragmentation. This paper focuses on this phenomenon and explains how it can be related to the initial conditions of the target.

Keywords:
Impact
Projectile
Fluid
Tank
Fragmentation model

1. Introduction

An important concern in risk management is the effect of projectile impact on a vessel holding a toxic liquid. Industrial tank catastrophic failure is an important concern in risk science. Whether it is a gaseous or liquid fluid, it is of interest to study the causes of such an event, then the consequences, and finally effects on humans and the environment.

1.1. Hydraulic ram

During the Apollo space project, catastrophic tank failure was studied [1] to understand the damage mechanism that would be induced when a meteorite impacts spacecraft fluid cells. Tests were carried out by impacting water tanks with hypervelocity projectiles (from 1301 m s^{-1} to 6400 m s^{-1}). In particular, researchers wanted to evaluate damage mechanisms caused by a hydraulic ram.

A hydraulic ram is a complex mechanism that involves a number of events: when a projectile enters a tank, a shock wave forms, and the high pressure and stresses near the entry point may cause cracks in the vessel. As the projectile traverses the fluid, high pressure is generated, and energy is imparted to the fluid through projectile drag. This increased energy sets the fluid in motion and forms a cavity. Fluid motion, cavity formation, and subsequent cavity collapse impose stresses on the tank walls. Finally, if the projectile has sufficient kinetic energy, it will exit the tank. As it exits, a local area of fluid is compressed, and cracks are produced around the exit hole. This phenomenon has been the subject of several investigations concerning the survivability of military aircraft fuel cells [2–5], and [6] and risk management [7,8]. The processes involved in a hydraulic ram are summarized in Fig. 1; two steps can be identified:

- At the time of impact there is a sudden and violent release of energy, which generates a shock wave;
- during the time that the projectile crosses the fluid, there is an additional exchange of energy that is not as strong but of longer duration than that at impact.

This short description demonstrates the complexity of physical mechanisms that contribute to a hydraulic ram.

1.2. Liquid ejection and instabilities

Various laboratories have worked on the resulting liquid instabilities [2,9–12]. Borg has performed a series of tests based on the same approach (projectile-target system), principally using an aluminum projectile (23.8 mm diameter) at velocities between 1630 m s^{-1} and 6000 m s^{-1} impacting a steel cylinder filled with TBP (tributylphosphate). His work concerns liquid expansion and instability. Borg managed to model the mechanism of liquid expansion and subsequent breakup caused by a hydraulic ram. His theory is based on conservation laws for expansion [13] and for breakup

* Corresponding author. Tel.: +33 4 66 78 27 66/01.
E-mail address: nicolas.lecysyn@ema.fr (N. Lecysyn).

Nomenclature

C_x	drag coefficient of projectile
C_{xj}	drag coefficient of liquid jet
d_j	liquid jet diameter (m)
d_p	projectile diameter (m)
d_v	average liquid fragment diameter (m)
ΔEc_p	kinetic projectile dissipation in the target (J)
Ec_{0j}	liquid ejection initial kinetic energy (J)
Ec_{breach}	breach growth energy (J)
$Ec_{overpressure}$	liquid overpressure energy (J)
F_j	liquid ejection force (N)
φ_1	analytical function relating drag force and physico-chemical parameters
φ_2	analytical function relating liquid ejection force and physico-chemical parameters
K	cavitation parameter
I	impact parameter
l_j	liquid jet length (m)
m_p	mass of the projectile (kg)
μ_l	fluid viscosity (Pa s)
P_0	initial static pressure at axis level of the projectile (Pa)
π_i	dimensionless parameter
Re	Reynolds number
R_p	Drag force on projectile (N)
ρ_{air}	air density (kg m^{-3})
ρ_l	fluid density (kg m^{-3})
ρ_p	projectile density (kg m^{-3})
σ_l	liquid surface tension (N m^{-1})
t	time (s)
u_{0j}	initial liquid ejection velocity (m s^{-1})
u_{p0}	projectile velocity before impact (m s^{-1})
u_p	projectile velocity after impact (m s^{-1})
V_j	liquid jet volume (m^3), depending on liquid jet diameter d_j (m)
V_p	projectile volume (m^3)

[14]. He focused particularly on a dimensional penetration study [2,11] that shows that projectile and liquid interaction phenomena do not depend on viscosity; he concluded that the phenomenon can be considered as inviscid. Moreover, he established a clear correlation between drag and liquid expansion. It is worth noting that the ratio of projectile diameter to target diameter was 25% to 33%. In this case the penetrating projectile was clearly the source of fluid ejection, as described in Fig. 2.

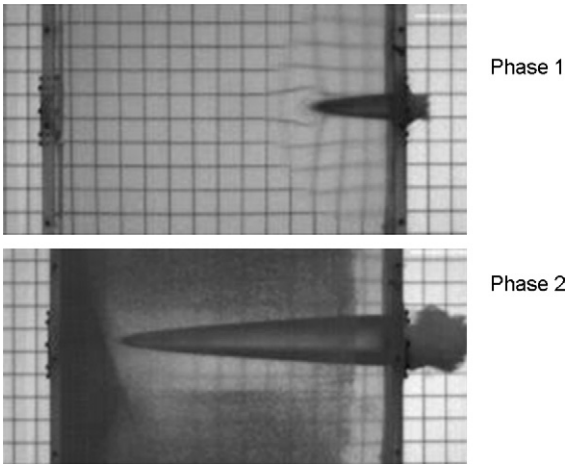

Fig. 1. Hydraulic ram phases [8].

2. Objectives

The aim of this work is to continue such studies focusing on vessels containing toxic liquids that could be the target of ballistic impacts. Full-scale tests were recently carried out at the CEG (Centre d'Etudes de Gramat) to assess the consequences of an impact on a tank filled with an industrial liquid. The first aim of this project was to study the hydraulic ram; in particular, to study the drag [7] and cavitation [8] phases. An original feature of our approach is that losses in projectile energy were determined without having sensors in the fluid. Another feature is that ratios of projectile to target diameters were less than 2%; this is a medium value compared to laboratory experiments (25% to 33% in [9–12]), and large-scale tests.

In this paper, we report

- measurements of liquid ejection such as fragmentation regime and fragments diameters and
- comparison with a hydraulic breakup model.

3. Experimental devices

Tests were performed to reproduce a projectile impacting a liquid-filled tank. A gun was used to accelerate a sabot device containing a small spherical projectile. To measure liquid fragmentation and subsequent evaporation, two devices were set up:

- a very high-speed frame recording device (4000 Hz) and
- a chemical-sensor mesh (1 Hz).

In this paper, chemical sensors do not play a role because only the first milliseconds of the phenomena are analysed; therefore, the chemical-sensor mesh is not described here.

Table 1 lists the 22 tests trials carried out during this study.

3.1. Test vessels

The experimental setup is presented in Fig. 3. A cylindrical steel vessel (diameter = 360 mm, height = 622 mm, volume = 60 L, thickness = 0.7 mm) was securely attached to two hangers, spaced at contact points between the vessel and two neighboring pseudovessels. To be representative of industrial storage, the liquid vessel was not completely filled (height of gas phase = 40 mm).

Vessels were commercial 60-L capacity barrels (Manutan). They were manufactured from steel of thickness 1 mm for the plane parts and thickness 0.6 mm for the side cylinders. The real volume of each barrel was about 63 L.

3.2. Solution properties

Two types of solutions were used in the experiments. Each contained urban water either with or without polyethylene glycol 400. Polyethylene glycol 400 is a liquid at ambient temperature and is a polymer characterized by a high viscosity. Binary mixtures (containing either 40% or 74% PEG mass fraction) are representative of common organic liquids that are stored in the chemical process industry (Fig. 4). The physico-chemical characteristics of the solutions are expected to influence the system's response to impact events.

Densities of aqueous solutions of polyethylene glycol 400 are given in the literature [15,16]. Thus, the properties of the aqueous solutions employed in these tests are located in the red part of Fig. 4.

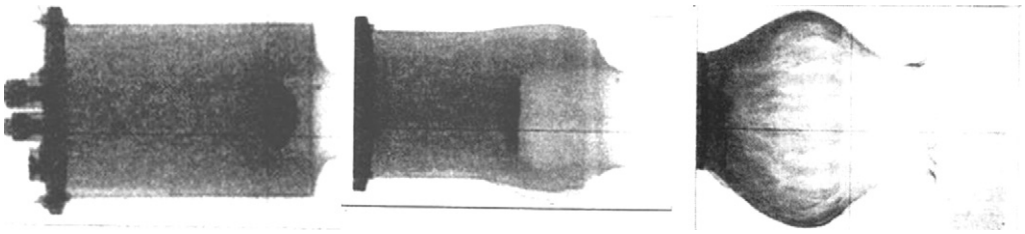

Fig. 2. Fluid ejection and instabilities [2].

Table 1
Experimental setup and trials.

u_{p0}[a] (m s^{-1})	Solution	Device	Camera/resolution (pix)	Comments
1125	Water + rhodamine	6 weighing devices 6 thermocouples 1 ultrasonic anemometer 1 anemometer 1 immersed piezoelectric pressure sensor 9.2.1	APX RS 1024*512 APX NB 5000 1024*512 APX Color 1024*512	Tests series 2005 Steel tank 60l
1148	Water + rhodamine + NH_4 + OH	24 electrochemical sensors 6 weighing devices 6 thermocouples 1 ultrasonic anemometer 1 anemometer 1 immersed piezoelectric pressure sensor	APX RS 1024*512 APX NB 5000 1024*512 APX Color 1024*512	
1167	Water + rhodamine + NH_4 + OH	24 electrochemical sensors 6 weighing devices 6 thermocouples 1 ultrasonic anemometer 1 anemometer 1 immersed piezoelectric pressure sensor 9.2.3	APX RS 1024*512 APX NB 5000 1024*512 APX Color 1024*512	
1193	Water + rhodamine	6 weighing devices 6 thermocouples 1 ultrasonic anemometer 1 anemometer 1 immersed piezoelectric pressure sensor 9.2.4	APX RS 1024*512 APX NB 5000 1024*512 APX Color 1024*512	
941	Water(2)	41 electrochemical sensors	APX 250k/1024*512	Tests series 2006
1255	Water + 10% NH_4 + OH (2)	1 ultrasonic anemometer 1 immersed piezoelectric pressure sensor	9.2.5	Steel tank 60l 9.2.6
1460	Water(2)			
971	Water + 10% NH_4 + OH + 40% PEG 400(2)			
1273	Water+ 10% NH_4			
963	Water + 10% NH_4 + 74% PEG 400(2)			
1215	Water(2)			
1241	Water(2)			
927	Water(2)			
978	Water + 40% PEG 400(2)			
1094	Water + 40% PEG 400(2)			
1255	Water	2 immersed piezoelectric pressure sensors	APX 250k/64*256 APX 250k/256*128 APX 250k/256*128	Tests series 2007 PC Tank(1) Cylindrical 166l
1255	Water	2 immersed piezoelectric pressure sensors 9.2.7	APX 250k/64*256 APX 250k/256*128 APX 250k/256*128 APX 250k/256*128	Tests series 2007 PC Tank(1) Cubic 181l
963	Water + 74% PEG	2 immersed piezoelectric pressure sensors 9.2.8	APX 250k/256*64 APX 250k/256*128 APX 250k/128*128	Tests series 2007 PC Tank(1) Cylindrical 166l

Table 1(*Continued*)

u_{p0}[a] (m s^{-1})	Solution	Device	Camera/resolution (pix)	Comments
1255	Water(2)	1 immersed piezoelectric pressure sensor 9.2.9	APX 120k/1024*512 APX 120k/1024*512 APX 250k/1024*512	Tests series 2007 Steel tank 60l 9.2.10
1273	Water + 40% PEG 400(2)		APX 120k/1024*512 APX 120k/1024*512 APX 250k/1024*512	
963	Water + 74% PEG 400(2)		APX 120k/1024*512 APX 120k/1024*512 APX 250k/1024*512	
1273	Water + 40% PEG 400(2)		APX 120k/1024*512 APX 120k/1024*512 APX 250k/1024*512	
	9.2.12	9.2.13	9.2.14	9.2.15

[a] PC: polycarbonate.

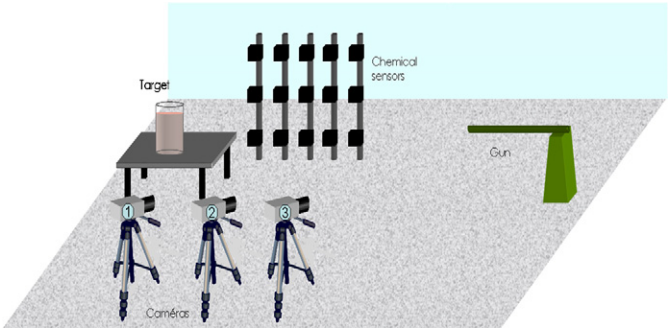

Fig. 3. Experimental setup.

3.3. Projectiles

The projectiles used for the impact tests were solid spheres whose diameters were assumed constant even after impact (13 mm). The projectile material was Denal, which is a tungsten alloy; the particle mass ranged from 20.1 g to 20.2 g. Each bullet was fired at a distance of 15 m from the vessel.

3.4. Optical apparatus

A high-speed framing technique has previously been applied to hydrodynamic studies of, for example, diesel jet breakup [17], water spray [18], water entry, and supercavitation [19,3]. In those studies the scene was illuminated by a background light, which was scattered by the jet. In our experiment, because of specific conditions due to the gun, the target was illuminated directly with three spotlights of 3500 W each. However, natural sunshine was the major source of light so, from one test to another, optical conditions were not the same. The field of view of each camera was within 2.5 m and the focal distance was chosen to provide complete coverage of the experimental field. Optical aberrations are estimated to be 2% of maximum full field. The use of a supersensitive 10 bit CMOS (complementary metal oxide semiconductor) was chosen for its ability to capture fast events [20]. The cameras were Photron Fast Cam APX 120 K, working at 4000 frames per second at full resolution (1024 × 1024 pixels).

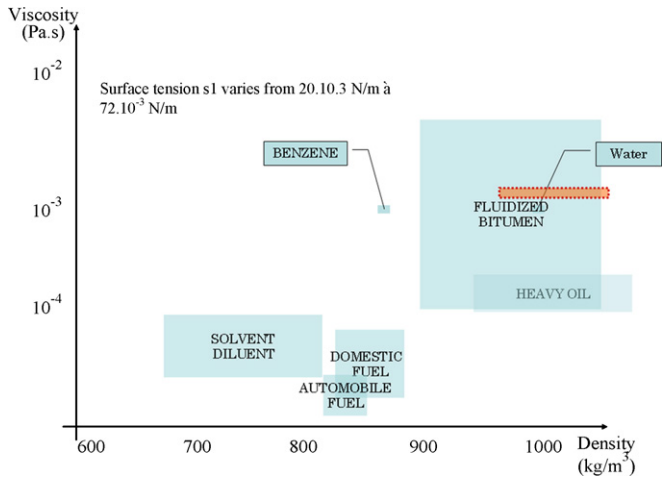

Fig. 4. Industrial solutions properties.

4. Experimental methods

Video sequences were processed to enhance the projectile displacement images [16]; postprocessing consisted of filtering, eroding, and thresholding of each image from the shotgun sequences.

Fig. 5 illustrates images to be processed, from which experimental information has been extracted such as

- projectile velocity before and after impact (phase 0) [7];
- liquid velocity and shape (phase 1);
- liquid fragment characteristic dimensions (phase 3).

4.1. Measurement of liquid shape and movement

Some specific algorithms have been developed [21] in order to get liquid ejection velocity. They first aim at extracting liquid jet image shape (in blank in Fig. 6) in order to get 2D coordinates. Coordinates are the intersection between liquid shape and a mesh (in blue).

4.2. Measurement of liquid fragments

Video sequences were processed to enhance the projectile displacement images [21]; postprocessing consisted of filtering, eroding, and thresholding of each image from the shotgun sequences.

Maximum Feret diameters have been computed (Fig. 7) on white blobs representing liquid fragments.

It is of interest to evaluate uncertainties; thus a measurement has been made at the beginning of each image sequence. As the projectile was crossing the field of view, its diameter has been measured, and related to its real dimensions.

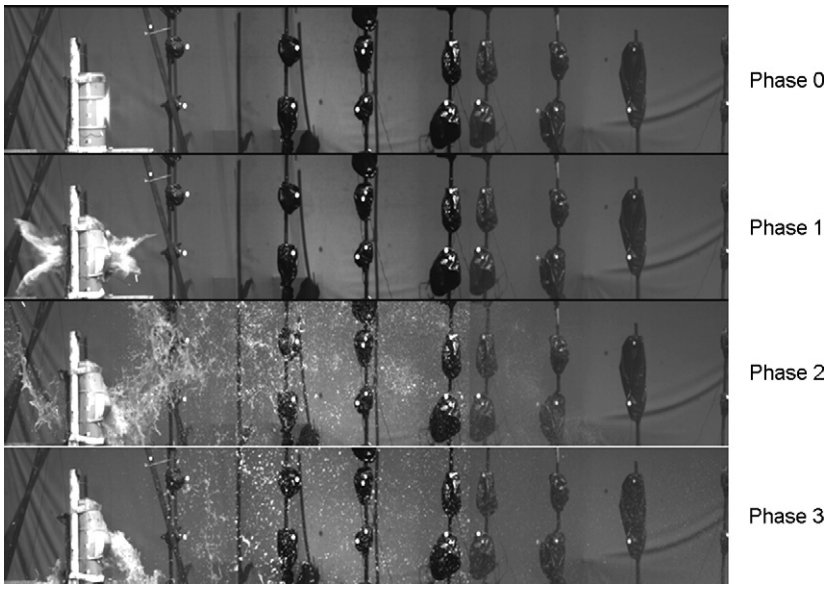

Fig. 5. Liquid ejection phases after impact.

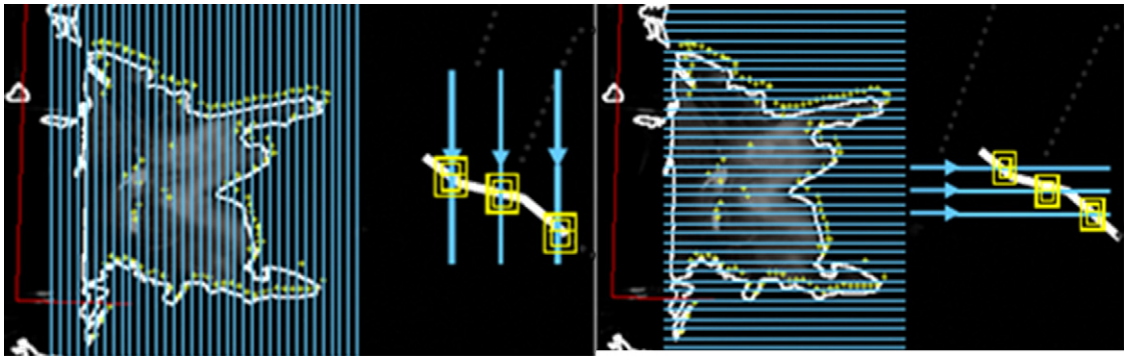

Fig. 6. Liquid jet 2D displacement field method.

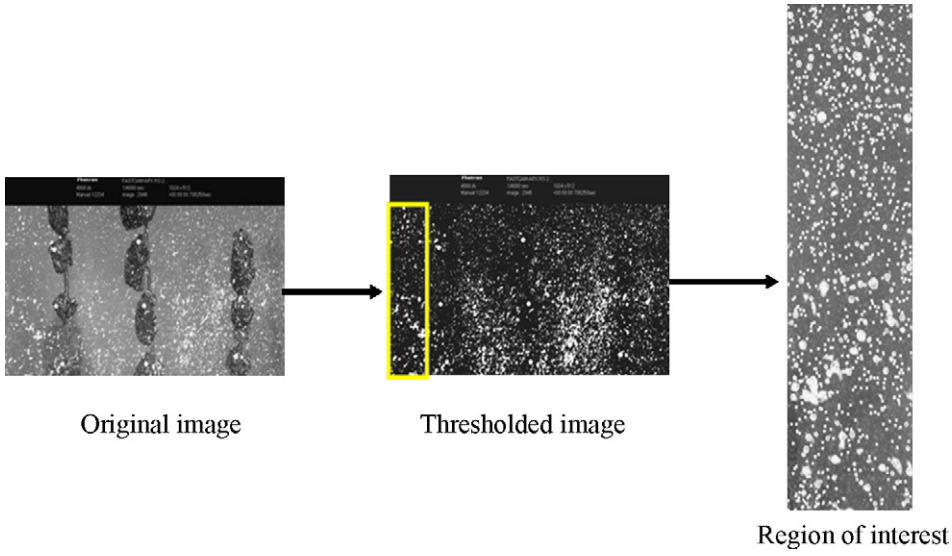

Fig. 7. Image thresholding.

$$\pi_1 = \frac{R}{\rho_l u_p^2 d_p^2} \cong C_x$$

$$\pi_2 = \frac{\mu_l}{\rho_l u_p d_p} = \frac{1}{\mathrm{Re}}$$

$$\pi_3 = \frac{P_0}{\rho_l u_p^2} \cong K$$

$$\pi_4 = \frac{\rho_l d_j u_j^2}{\sigma_l} = We$$

$$\pi_5 = \frac{u_p}{u_j}$$

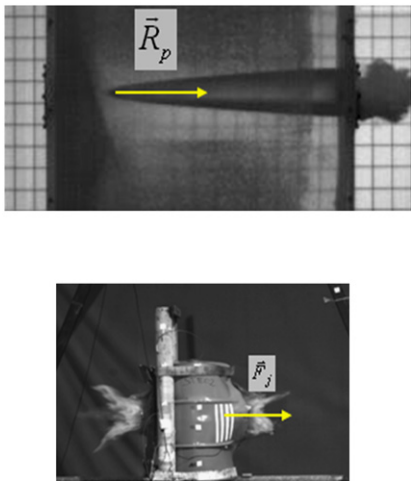

Fig. 8. Dimensional study.

The average difference between measures done on image and real projectile dimensions represents 6.7%, with an error due to image resolution (3 mm per pixel).

5. Results and modeling

5.1. Dimensional study

Solid and fluid dynamics relations and the theory of liquid fragmentation allow to the two functions φ_1 and φ_2 to define respectively the projectile drag (R_p) and the liquid ejection force (F_j), as illustrated in Fig. 8:

$$R_p = \varphi_1(u_p, \rho_l, \mu_l, d_p, \rho_p, P_0)$$

$$F_j = \varphi_2(\rho_l, u_j, d_j, \sigma_l)$$

So nine parameters (projectile velocity, diameter and density; liquid density, viscosity, surface tension, and hydrostatic pressure; ejection velocity; and liquid jet diameter) and three fundamental dimensions ([M], [L], [T]) characterize the problem.

Applying the Vashy–Buckingham principle, and after having analyzed the physical phenomena, thanks to image sequences (Section 4), we propose six non-dimensional parameters:

$$\begin{aligned}
\pi_1 &= \frac{R_p}{\rho_l u_p^2 d_p^2} \cong C_x \\
\pi_2 &= \frac{\mu_l}{\rho_l u_p d_p} = \frac{1}{Re} \\
\pi_3 &= \frac{P_0}{\rho_l u_p^2} \cong K \\
\pi_4 &= \frac{\rho_l d_j u_{0j}^2}{\sigma_l} = \mathrm{We} \\
\pi_5 &= \frac{u_p}{u_j} \\
\pi_6 &= \frac{C_x \rho_l u_{p0} t}{\rho_p d_p} = I
\end{aligned} \tag{2}$$

- π_1 is the projectile drag, which is related to projectile deceleration due to liquid,
- π_2 is related to the Reynolds number, that is to say the flow regime around the projectile,
- π_3 the cavitation parameter proposed by [22], which predicts the cavitation phenomenon in the wake of the projectile,
- π_4 is the Weber number, giving information about the liquid fragmentation regime,
- π_5 is the velocity ratio between projectile and liquid ejection,
- π_6 is the impact parameter proposed by [1], which predicts projectile velocity decay.

This set of parameters, which depend on physico-chemical characteristics, static or dynamic initial conditions, allows an analytical approach.

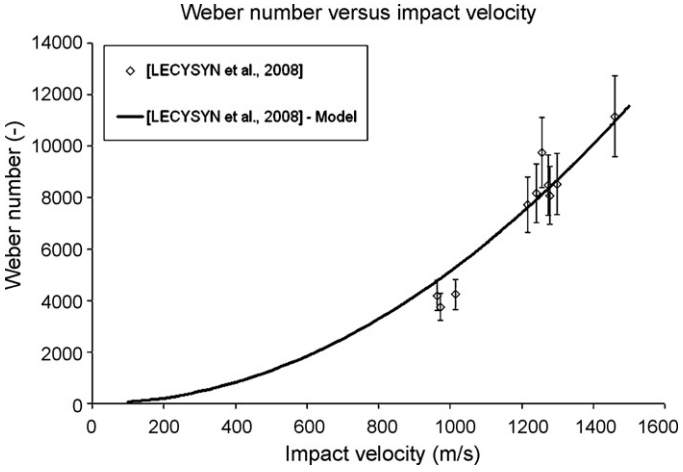

Fig. 9. Weber number model and experimental values.

5.2. Energy balance

The target tank is initially at rest; its catastrophic failure is exclusively due to projectile kinetic energy supply to the system. As the energy balance of target/projectile is well known analytically [22], it is of interest to set up another energy balance for liquid ejection. Borg has proposed in [6] a analytical expression, which can be adapted to this study:

$$\Delta Ec_p = Ec_{0j} + Ec_{\mathrm{breach}} + Ec_{\mathrm{overpressure}} \tag{3}$$

As the liquid is ejected, a shock wave has been totally dissipated in the liquid [8], and breach is already opened [23]. Consequently, both the terms Ec_{breach} and $Ec_{\mathrm{overpressure}}$ are neglected.

It is possible to write relation 3 as

$$\frac{1}{2} m_p (u_{p0}^2 - u_p^2) = \frac{1}{2} \rho_l . V_j(d_j) . u_{0j}^2 \tag{4}$$

It is also possible to predict the liquid ejection velocity u_{0j}.

u_{p0} and u_p are related to the impact parameter I [22] thanks to the relation

$$\frac{u_p}{u_{p0}} = \frac{1}{1 + (3/4)I} \tag{5}$$

d_j is related to the cavitation parameter K, impact parameter I, projectile diameter d_p, and projectile C_x [8]:

$$d_j = \sqrt{\frac{C_x(1+K)}{K(1 - 0.132\sqrt{K})}} . d_p \tag{6}$$

The Weber number can expressed as

$$\mathrm{We}_j = \frac{4 m_p (1 - I^2)}{\sigma_j \pi . l_j . \sqrt{(C_x(K))/(K(1 - 0.132\sqrt{K}))} . d_p} . U_{p0}^2 \tag{7}$$

Fig. 10 illustrates the good correlation between experimental values and model for six points in the velocity range up to

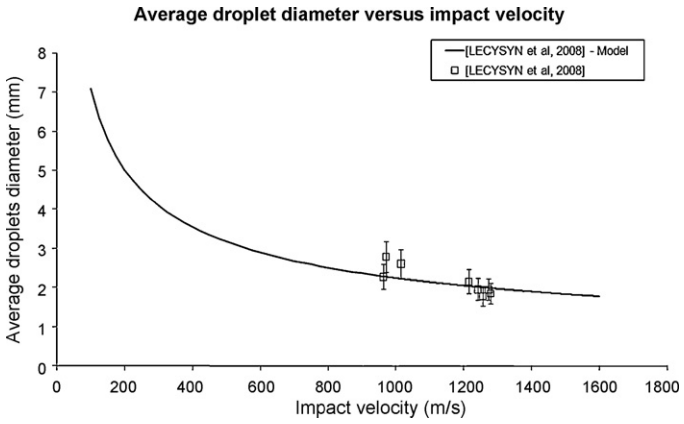

Fig. 10. Average droplet diameters.

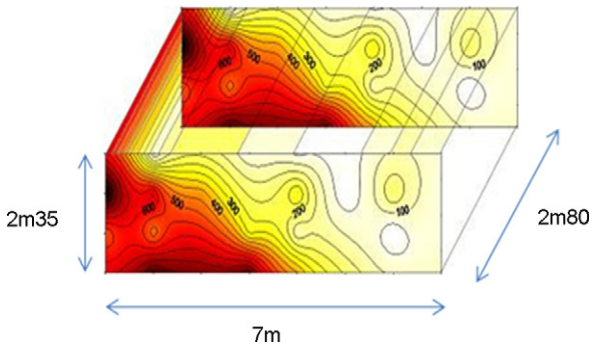

Fig. 12. Volume containing vapor cloud. Concentrations values are in ppm.

1200 m s^{-1}. Four other points do not fit rather well with theoretical curve; however, they follow the trend.

It is worth noting that experimental Weber numbers are above 1000, which is representative of catastrophic liquid primary fragmentation [24].

It is therefore of interest to focus the study on liquid droplets created from this primary liquid fragmentation. We utilize an empirical law [25] developed for hydraulic nozzles:

$$\frac{d_v}{d_j} = 1.9\,We^{-0.25} + 0.315\left(\frac{\rho_{air}}{\rho_l}\right)^{1,5} C_{xj} We^{-0.125} \ln\frac{d_j}{d_v} \tag{8}$$

Injecting (7) in (8), it gives

$$\frac{d_v}{d_j} = 1.9\left(\frac{4m_p(1-I^2)}{\sigma_j \pi . l_j . \sqrt{(C_x(K))/(K(1-0.132\sqrt{K}))}.d_p}.U_{p0}^2\right)^{-0.25} + 0.315\left(\frac{\rho_{air}}{\rho_l}\right)^{1,5} C_{xj} \times \left(\frac{4m_p(1-I^2)}{\sigma_j \pi . l_j . \sqrt{(C_x(K))/(K(1-0.132\sqrt{K}))}.d_p}.U_{p0}^2\right)^{-0.125} \ln\frac{d_j}{d_v} \tag{9}$$

Fig. 10 shows that this model is validated by experimental data for five points, and three other points follow the trend.

This graphical representation shows that the higher the impact velocity, the smaller the average liquid fragment diameter. From this average diameter value, a log-normal law [26] has been computed and compared to diameters distribution in the liquid jet (Fig. 11).

Experimental values are not represented for diameters less than 3 mm, which is the image resolution limit, and for diameters more than 31 mm we chose not to consider these kinds of liquid fragments as droplets. The log-normal law does not fit ideally with experimental values, which is probably due to several reasons:

- the lack of data in the range of 0–3 mm;
- uncertainties (Section 4.2);
- errors made by the image processing method, which evaluate a 3D phenomenon from a 2D measure.

6. Discussion

This discussion is based on Fig. 5. First of all, it has been observed that the breach in the target tank is very important, compared to tank dimensions; [10] has measured a breach height equivalent to the target height, and a maximum breach area reaching within 1 ms 60% of target cross-sectional area. It is obvious that in case of a

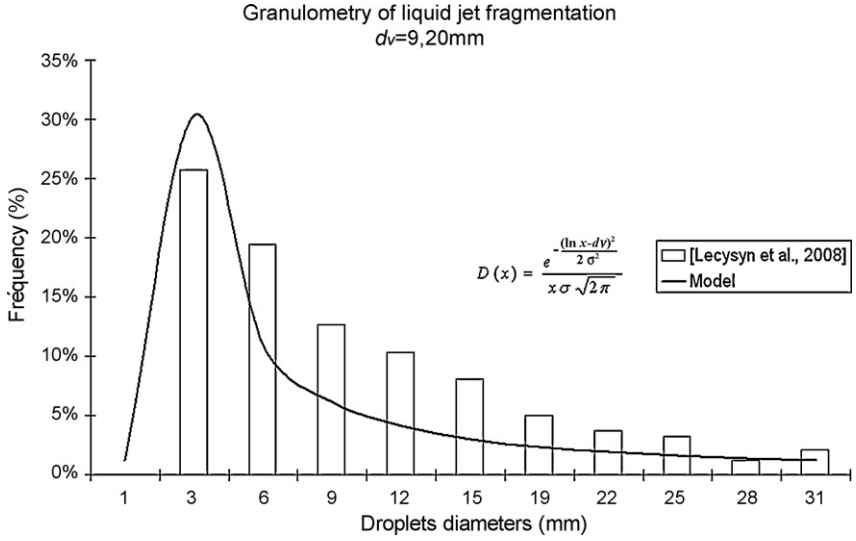

Fig. 11. Diameter distribution.

full-scale industrial tank, which can reach twenty meters, the hole created at impact by projectile would be very small to tank dimensions. We can also imagine that a small part of the liquid would be ejected. Numerical simulations (using source term proposed in this paper) could be a first response element to evaluate the amount of liquid ejected. Afterwards it is very probable that about 95% of the liquid contained above the breach would leak due to gravity, which can be modeled by Bernoulli's relation.

Secondly, it is assumed that droplets (diameter less than 3 mm) that are not detected by the camera probably do not hit the floor and evaporate. In the study proposed by [23], a mechanism has been proposed for liquid evaporation in two steps:

- Vapor cloud formation: droplet initial velocities of 60 m s^{-1} (average) favor vaporization, and the cloud is generated in the liquid jet axis with a concentration gradient as illustrated in Fig. 12.
- Vapor dispersion: local turbulence contributes to vapor cloud growth.
- The third mechanism is due to liquid droplets and leakage, which form a liquid sheet on the ground, and evaporate.

7. Conclusions

Tests were performed to analyze the consequences of high-speed impacts of projectiles onto a tank filled with a toxic liquid. Such an impact results in catastrophic failure of the vessel and leads to liquid ejection and fragmentation. A dimensional study emphasizes contribution of six parameters, which for this study have specific values:

$$\begin{aligned} &C_x = 0.45 \\ &Re > 10^6 \\ &K = 10^{-6} \\ &\mathrm{We} > 1000 \\ &\frac{u_\mathrm{p}}{u_\mathrm{j}} = 30 \\ &I = 1 \end{aligned} \tag{10}$$

For this set of experimental values, the models have been validated by experimental data and lead to the following conclusions (Fig. 9):

- There is a turbulent flow regime around the projectile as it crosses the target; it decelerates from 30% to 40%, this assumption has been proposed and discussed in [7].
- Cavitation is always occurring in the wake of the projectile, as described in [28].
- Liquid ejection leads to catastrophic fragmentation into droplets that have a velocity thirty times less than impact velocity, and have an average diameter of 9 mm.

Fig. 4 shows that this analytical approach is correct for a small range of physico-chemical values, compared to the largest one that exists in the chemical industry. Moreover, only one type of target tank was tested; it would be of great interest to manage other tests at different scales. However, the cost of such an experimental approach could be difficult to support. To optimize it, numerical study could achieve interesting results. Such a study is beginning [27].

The ultimate goal of this project is to obtain an integrated description from projectile impact to consequences in terms of container failure, catastrophic liquid discharge, and final breakup, which would lead to evaporation and atmospheric dispersion (cloud concentrations).

Acknowledgements

The authors are grateful to DGA (Délégation Générale pour l'Armement) for their financial support, and thank the CEG (Centre d'Etudes de Gramat) for their efficient help during tests series.

References

[1] F. S. Stepka, C. Lewis, R. Morse, R.P. Dengler, Investigation of Characteristics of Pressure Waves Generated in Water Filled Tanks Impacted by High-Velocity Projectiles, NASA TECHNICAL NOTE NASA TN D-3143,1965.
[2] R.E. Ball, Structural Response of Fluid-containing Tank to Penetrating Projectiles (Hydraulic ram)—A Comparison of Experimental and Analytical Results, 1976, 105 p., NPS-57Bp76051.
[3] P.D. Holm, Hydraulic Ram Shock Wave and Cavitation Effects on Aircraft Fuel Cell Survivability, 1973, p. 80.
[4] E.A. Lundstrom, W.K. Fung, Fluid Dynamic Analysis of Hydraulic Ram Iii (Result of Analysis), 1976, JTCG/AS-74-T-015:136.
[5] L.S. Mueller, Experimental Investigation of Hydraulic Ram, 1974, 46 p.
[6] D. Townsend, N. Park, P.M. Devall, Failure of fluid dilled structures due to high velocity fragment impact, International Journal of Impact Engineering 29 (2003) 723.
[7] N. Lecysyn, A. Dandrieux, F. Heymes, P. Slangen, L. Munier, E. Lapébie, C. Le Gallic, G. Dusserre, Preliminary study on ballistic impact on an industrial tank: projectile velocity decay, International Journal of Loss Prevention in the Process Industries 21 (6) (2008) 627–634.
[8] N. Lecysyn, A. Dandrieux, F. Heymes, L. Aprin, P. Slangen, L. Munier, E. Lapébie, C. Le Gallic, G. Dusserre, Experimental study of hydraulic ram effect on a liquid storage: analysis of overpressure and cavitation induced by a high-speed projectile. J. Hazard. Mater.under review (2009).
[9] J.P. Borg, D. Grady, J.R. Cogar, Instability and fragmentation of expanding liquid systems, International Journal of Impact Engineering 26 (65) (2001).
[10] J.P. Borg, J.R. Cogar, S.L. Ference, Fluid Dispersion from a Thin Walled Container Impacted by a Spherical Projectile Emerging Technologies in Fluid, PVP-414-1, 2000.
[11] J.P. Borg, J.R. Cogar, S. Tredways, J. Yagla, M. ZwienerR, Damage Resulting from High Speed Projectile Liquid Filled Metal Tanks, 2001.
[12] J.P. BORG, J.R. Cogar, Comparison of average radial expansion velocity from impacted liquid filled cylinders, International Journal of Impact Engineering 34 (2007) 1020.
[13] R.W. Gurney. The initial velocities of fragments from bombs, shells and grenades, BRL Report 405, 1943.
[14] D.E. Grady, The spall strength of condensed matter, Journal of the Mechanics and Physics of Solids 36 (1988) 353.
[15] A. Yurquina, M.E. Manzur, P. Brito, R. Manzo, M.A.A. Molina, Physicochemical studies of acetaminophen in Water-Peg 400 systems, Journal of Molecular Liquids 133 (2007) 47.
[16] S. Kirincic, C. Klofutar, Viscosity of aqueous solutions of poly(ethylene glycol)S at 298.15K, Fluid Phase Equilibria 155 (1999) 311.
[17] N. Chigier, Optical imaging of sprays, Progress in Energy and Combustion Science 17 (1991) 211–262.
[18] M. Amielh, J-D. Giorgetto, J-P. Heichelbech, A. Tchiftchibachian, Granulometrie Et Velocimetrie De L'atomisation Primaire D'un Jet Liquide Par Analyse D'image, 10ème Congrès Francophone de Techniques Laser 19–22 Septembre 2006, Toulouse - Toulouse, France, 2006.
[19] H.H. Shi, I. Motoyuki, T. Takuya, Optical observation of the supercavitation induced by high-speed water entry, Transactions of the ASME 122 (2000) 806–810.
[20] R. Schmidt, M. Hugenschmidt, W. Baca, Kurzzeitkinematographie Mit Digitaler Kameratechik–Technologie Des Caméras Numériques Utilisée En Cinématographie Ultrarapide, DPG-Frühjahrstagung, - Kiel, BRD, 2.3,2004.
[21] N. Lecysyn, F. Heymes, A. Dandrieux, P. Slangen, G. Dusserre, L. Munier, E. Lapébie, C. Le Gallic, Experimental Investigation of a Catastrophic Tank Failure with a High Speed Video Recorder. Image Processing and Hydrodynamic Characterization of the Liquid Jet, 12th International Symposium Loss prevention and Safety Promotion in the Process Industries, Edinburgh, Scotland, Topic 4, Paper 212, 2006.
[22] R.T. Knapp, J.W. Daily, F.G. Hammit, Cavitation (1970) 196–197.
[23] F. Heymes, A. Bony-Dandrieux, N. Lecysyn, R. Spinelli, G. Dusserre, Etude De La Dispersion Atmosphérique D'un Polluant Lors De La Destruction D'un Stockage Rapport Final. Convention ARMINES No 40827:87,2006.
[24] R.I. Nigmatulin, N.A. Gumerov, N.H. Zuong, Transient heat and mass transfer near drops and bubbles, phaseinterface phenomena in multiphase flow, in: G. Hewitt, F. Mayinger, J. Riznic (Eds.), Hemisphere, 1991.
[25] J.O. Hinze, Turbulence, 1975, 790 p., ISBN 0070290377.
[26] M.R. Vetrano, J. Gauthier, P. Van Beek, J.M. Buchlin, characterization of a non-isothermal water spray by global rainbow thermometry, Experiments in fluids 40(1) (2005) 15–22.
[27] N. Lecysyn, L. Aprin, A. Dandrieux, F. Heymes, L. Munier, G. Dusserre, Preliminary investigations on hydraulic ram. J. Hazard. Mater.under review (2009).
[28] F. Petitpas, J. Massoni, R. Saurel, E. Lapebie, L. Munier, Diffuse interface model for high speed cavitating underwater systems, International Journal of Multiphase Flow 35 (8) (2009) 747–759.